Appl. Phys. A 89, 213–219 (2007)
DOI: 10.1007/s00339-007-4093-7
Applied Physics A
Materials Science & Processing

J.-L. WANG[1,✉]
Y.-S. LAI[2]
B.-S. CHIOU[1]
C.-C. CHOU[3]
C.-C. TSAI[1]
T.G.-Y. LEE[1]
H.-C. CHENG[1]

Crystallinity and electrical properties of (Pb, Sr)TiO_3 films enhanced by laser-assisted low-thermal-budget annealing

[1] Department of Electronics Engineering and Institute of Electronics, National Chiao Tung University, 1001 Ta Hsueh Rd., Hsinchu 30050, Taiwan R.O.C.
[2] Department of Materials Science and Engineering, National United University, Miaoli 36003, Taiwan R.O.C.
[3] Department of Mechanical Engineering, National Taiwan University of Science and Technology, Taipei 10607, Taiwan R.O.C.

Received: 12 March 2007/Accepted: 3 May 2007
Published online: 20 June 2007 • © Springer-Verlag 2007

ABSTRACT The physical and electrical properties of (Pb, Sr)TiO_3 (PSrT) films annealed by various techniques are systematically investigated in this study. The crystallinity and ferroelectricity of PSrT films can be enhanced by excimer laser annealing (ELA), but the effect only works on the upper region of films. On the other hand, PSrT films treated by rapid thermal annealing (RTA) can also improve crystallinity and ferroelectricity. However, the leakage current of films is seriously increased due to defects and interfacial diffusion induced by post-RTA at high temperature. As a result, the laser-assisted two-step annealing (post-ELA + RTA) is proposed in this work. It is found that PSrT films treated by post-ELA + RTA show improved crystallinity, better ferroelectric properties, higher dielectric constant, and lower leakage currents, which bring out the longer lifetime and higher breakdown field.

PACS 77.84.-s; 81.40.Ef; 42.62.-b

1 Introduction

(Pb, Sr)TiO_3 (PSrT) has received much attention lately for memory, sensor, frequency tuning devices, and microwave applications due to its large electric-field-dependent dielectric constant and composition-dependent Curie temperature [1–6]. The PSrT film is constituted by a solid solution of $PbTiO_3$ (PTO) and $SrTiO_3$ (STO). The Curie temperatures (T_c) of PTO and STO are 490 °C and −220 °C, respectively. Consequently, PTO and STO films, at room temperature, exhibit a tetragonal structure (ferroelectric phase) and a cubic structure (paraelectric phase). The effects of lead (Pb) substituted by strontium (Sr) in the PTO film decrease crystallization temperature and offer a good control of the dielectric properties at room temperature [1, 2].

Ferroelectric films usually require low-temperature processes for IC and MEMS applications to prevent the formerly-fabricated structure from thermal damage. Nevertheless, depositions of ferroelectric lead-titanate films, such as Pb(Zr, Ti)O_3 (PZT), are typically conducted at high-temperatures (> 600 °C) to obtain good crystallinity of a perovskite structure [7]. The high-temperature (> 490 °C) process will result in the volatilization of lead oxide (Pb-O compounds) in lead-titanate-based thin films [8, 9], which in turn affects the film composition and degrades the electric properties of ferroelectric device. Thus, a low-thermal budget process, a relatively low-temperature process with short thermal-duration, is certainly required for the preparation of PSrT thin films.

In this work, PSrT films were prepared at 200 °C using the pulsed-laser deposition (PLD) technique. The crystallinity of films is improved by rapid thermal annealing (RTA) or laser-assisted two-step annealing. Although the process temperature is high, RTA has been proposed to reduce the total thermal budget for ferroelectric films due to its short process time [10, 11]. The excimer laser annealing (ELA) is also very attractive in terms of selective annealing area and local high-temperature heating within very short time, which is utilized in the production of low-temperature poly-silicon (LTPS) thin film transistor (TFT) [12, 13]. However, the influence of ELA is only on the surface of ferroelectric films [11, 14–16]. Thus, the laser-assisted two-step annealing (i.e., the combination ELA and subsequent RTA) may become a promising technique to improve the crystallinity and electrical properties of PSrT films and the results will be addressed in this work.

2 Experimental procedures

A multilayer of Pt/PSrT/Pt/Ti/SiO_2/Si was used to simulate the structure of a capacitor over a bit-line (COB). The Pt/Ti films with thicknesses of 100/4 nm were subsequently sputtered onto the SiO_2/Si as the bottom electrode/adhesion layer. PSrT films with 120 nm in thickness were deposited by a KrF ($\lambda = 248$ nm, pulse width = 25 ns) pulsed-laser deposition (PLD) system (LPX 210i, Lambda Physik). A set of optical lenses was used to focus the excimer laser beam onto the $(Pb_{0.6}, Sr_{0.4})TiO_3$ target, prepared with conventional ceramic fabrication process [17]. In the process of PLD PSrT films deposition, the target to substrate distance was 4 cm. The deposition temperature and the ambient oxygen pressure (P_{O_2}) were 200 °C and 80 mTorr. The laser pulse rate and the average laser energy fluence (LEF) were 5 Hz and 1.55 J/cm^2 per pulse, respectively.

The as-deposited PLD PSrT thin films were post treated by rapid thermal annealing (post-RTA) (JetFirst Processor,

✉ Fax: +886-3-5738343, E-mail: joewang666@gmail.com

Jipelec) with the following conditions. The ambient oxygen gas flowing rate was 50 sccm. The process temperatures were 450 or 600 °C. The heating rate is programmed as 30 °C/s or 50 °C/s, respectively. The duration was 60 s. Furthermore, the as-deposited films were also annealed by laser-assisted two-step annealing: post-excimer laser annealing (post-ELA) and subsequent RTA (post-ELA + RTA). After the modulation of optical lens of the KrF excimer laser system, the post-ELA was processed with the following conditions. The substrate temperature was 300 °C. The P_{O_2} was 80 mTorr. The laser pulsed rate was 1 Hz. The average LEF was 47.6–105.6 mJ/cm^2 per pulse. The number of laser pulses was 40–180 pulses. The subsequent RTA was conducted at 450 or 600 °C in oxygen ambience for 1 min.

The surface morphology of PSrT films were examined by field emission scanning electron microscopy (FESEM) (S-4000, Hitachi). The crystallinity of the film was analyzed by X-ray diffractometer (XRD) (D5000, Siemens, using Cu K_α, $\lambda \sim 0.154$ nm) and glancing incident angle X-ray diffraction (GIAXRD) machine (D/MAX2500, Rigaku, using Cu K_α, $\lambda \sim 0.154$ nm) with a fixed incident angle of 2°. Cross-sectional transmission electron microscopy (TEM) (JEM-2000FX, JEOL, using the electron acceleration voltage of 200 kV) samples were fabricated by standard sample preparation techniques with tripod polishing and ion milling using the Gatan PIPS system operated at 3 kV. The combination of a semiconductor parameter analyzer (4156C, Agilent Technologies) and a probe station was used to measure the leakage current (I–V) characteristics. The testing voltage was biased on the top electrode, and the bottom electrode was grounded. A capacitance–voltage (C–V) analyzer (Package 82 system C-V 590, Keithley) was also used to measure C–V curves at 100 kHz.

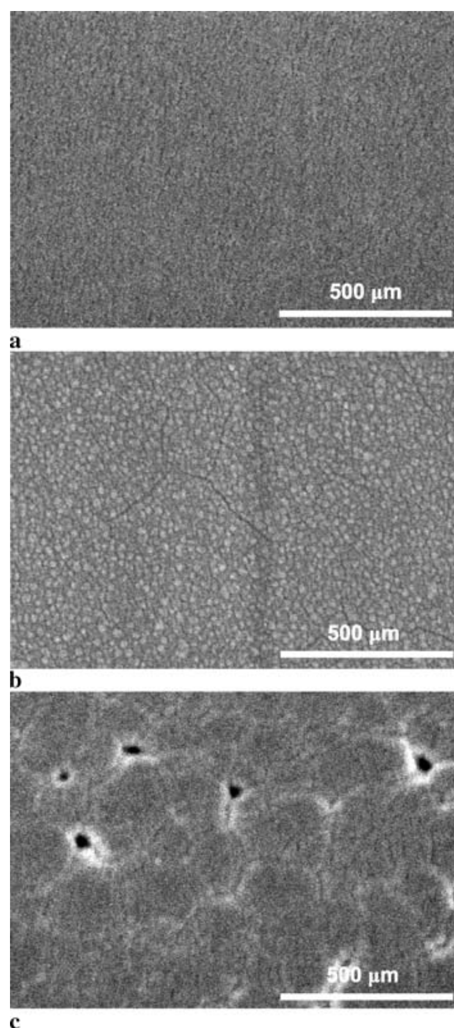

FIGURE 1 SEM surface morphologies of PLD PSrT films (**a**) un-annealed and post-rapid thermal annealed (post-RTA) at (**b**) 450 °C and (**c**) 600 °C

3 Results and discussion

3.1 *Effects of RTA on PSrT films*

Figure 1 shows the SEM surface morphologies of PLD PSrT films before and after rapid thermal annealing (RTA) at 450 °C and 600 °C. The un-annealed films reveal a smooth and dense surface. The grain clusters of films after RTA at 450 °C are not significant. However, after RTA at 600 °C, the surface reveals apparent grain clusters and pin holes. The pin holes themselves would act as defects. It suggests that the annealing time (60 s) is too short to promote grain growth. However, the longer annealing time could result in severe Pb-O volatilization and interfacial diffusion at high temperature [8–11].

Figure 2 presents XRD patterns of un-annealed and post-RTA films. The un-annealed films are amorphous. In contrast, the post-RTA ones exhibit obvious diffraction peaks of $(Pb_{1-x}Sr_x)TiO_3$ perovskite structures [1–3, 6]. The diffraction peaks are indexed as (100), (110) and (211) orientations and their intensities increase as the annealing temperature increases. The crystalline PSrT films are observed at such low annealing temperature (450 °C) because (i) the addition of strontium induces a lower crystallization temperature of PSrT than that of PZT [1, 10, 11], and (ii) the PLD technique can preserve the crystalline phase and stoichiometric ratio of the target material at low substrate temperature [17].

Figure 3 shows the capacitance versus electric field (C–E) characteristics of the un-annealed and post-RTA PSrT films. The figure presents the typical C–E hysteresis characteristics of ferroelectric materials. The capacitance shows a maximum value at negative bias when the applied field sweeps from +200 kV/cm to −200 kV/cm. However, the maximum capacitance appears at positive bias when the applied field sweeps in the reverse direction. It is argued that the asymmetric C–E loops can be possibly due to different electrical characteristics at the top and bottom interfaces. In our case, the bottom and top electrodes are the same material (i.e., Pt). The asymmetric C–E loop may be associated with the interfacial asymmetry induced by thermal processes (i.e., the top and bottom electrodes are subjected to different thermal processes) [18], and/or the different electrode areas (i.e., the area of the bottom electrode is larger than that of the top electrode, as defined by shadow mask). The un-annealed film does not exhibit a C–E hysteresis loop, which presents the paraelectric-like characteristic. On the contrary, it indicates that the distinct C–E hysteresis loops and larger capacitance can be obtained after RTA at higher temperatures. This result suggests that the ferroelectricity of PSrT films is evidently improved by post-RTA, which is consistent with the observation of XRD (Fig. 2).

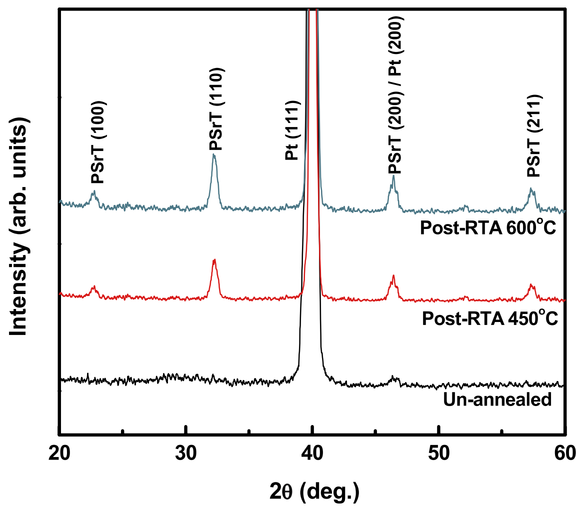

FIGURE 2 X-ray diffraction patterns of PSrT films un-annealed and post-RTA at 450 and 600 °C

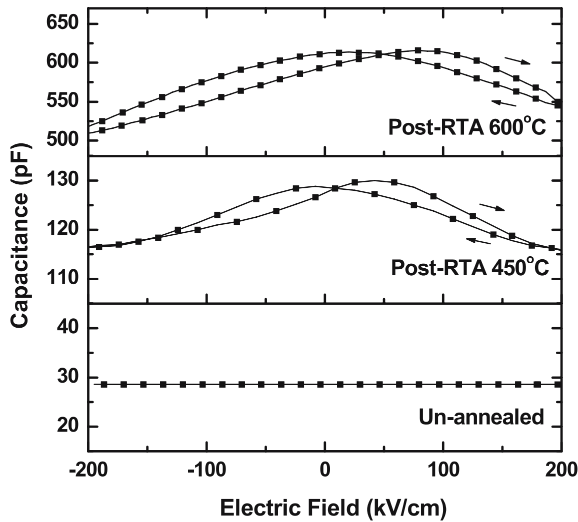

FIGURE 3 Capacitance versus electric field (C–E) hysteresis loops of PSrT films un-annealed and post-RTA at 450 and 600 °C

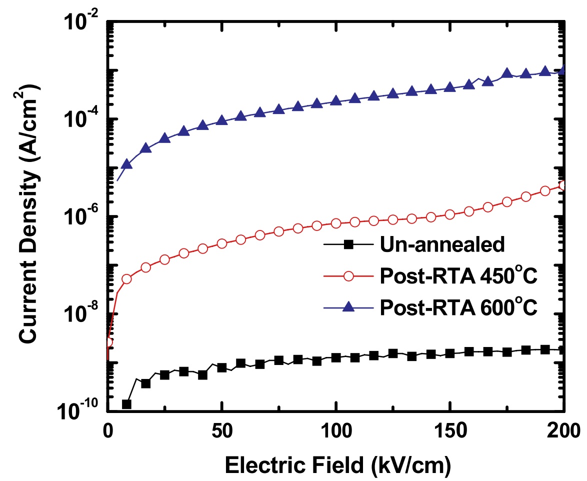

FIGURE 4 Current density versus electric field (J–E) characteristics of PSrT films un-annealed and post-RTA at 450 and 600 °C

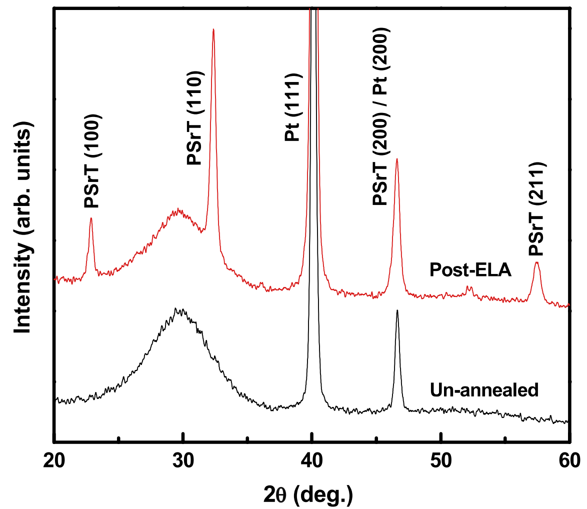

FIGURE 5 Glancing incident angle X-ray diffraction (GIAXRD) patterns of PSrT films un-annealed and post-excimer laser annealed (post-ELA) at laser energy fluence (LEF) of 47.6 mJ/cm^2 per pulse with 120 pulses

Figure 4 shows the current density versus electric field (J–E) characteristics of Pt/PSrT/Pt capacitors under positive bias. It is found that the leakage current is seriously increased when the RTA temperature increases. These worse J–E characteristics could be linked to the defects (i.e., grain boundaries in Fig. 1) and interfacial diffusion (addressed later) induced by post-RTA. As mentioned above, it is clear that the crystallinity and ferroelectricity of PSrT films can be evidently improved by post-RTA. Nevertheless, the deteriorative J–E characteristics of post-RTA films will limit the application in memory devices.

3.2 *Effects of ELA on PSrT films*

The physical properties of ferroelectric films after excimer laser annealing are dependent on several parameters (i.e., the laser pulsed rate, the average LEF, and the number of laser pulses) [11–16]. Figure 5 presents the GIAXRD pattern of PSrT films un-annealed and post-ELA at LEF of 47.6 mJ/cm^2 per pulse with 120 pulses. The distinct diffraction peaks of post-ELA films possibly indicate that the film is transformed from amorphous to partly perovskite structures after ELA (confirmed by TEM analysis later on). However, the $\theta/2\theta$ XRD patterns reveal no observable change in PSrT films with/without post-ELA (addressed later). As a result, it suggests that the crystallinity of the upper region of PSrT films is markedly enhanced by post-ELA since the radiation of KrF laser is mostly absorbed in a thin surface layer [14, 16]. This result also implies that the corresponding electrical properties of films can be affected by post-ELA, which will be discussed later. Since it is difficult to transform the whole PSrT films into perovskite structures by post-ELA, a further heat treatment is required after ELA, such as a subsequent RTA.

3.3 *Effects of laser-assisted two-step annealing on PSrT films*

As mentioned above, there are some advantages and drawbacks of films after RTA or ELA. Therefore, the laser-assisted two-step annealing (i.e., the combination of

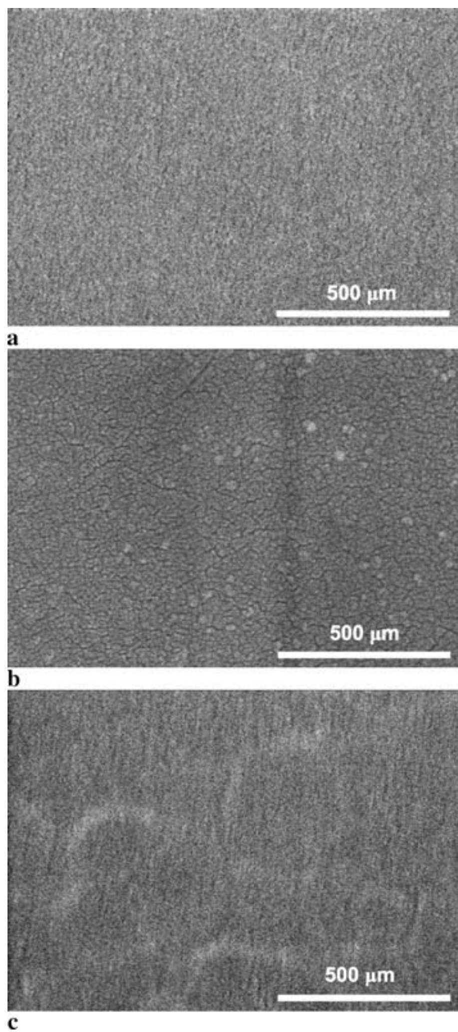

FIGURE 6 SEM surface morphologies of PLD PSrT films post-ELA and subsequent RTA (post-ELA + RTA) at (**b**) 450 °C and (**c**) 600 °C

post-ELA and subsequent RTA) is conducted. The two-step annealing is proposed to improve the crystallinity and electrical properties of PSrT films. Figure 6 shows the SEM surface morphologies of films after ELA and subsequent RTA (post-ELA + RTA) at 450 °C and 600 °C. The post-ELA films reveal a dense surface, which is analogous to that of the un-annealed one. The uniform and small grain clusters can be obtained for post-ELA + RTA films at 450 °C. Post-ELA + RTA films at 600 °C exhibit a smooth surface with some light imprints. The change of surface morphologies implies that the microstructure of films could be affected by different annealing conditions.

Figure 7 presents XRD patterns of films un-annealed, post-ELA, and post-ELA + RTA at 450 and 600 °C. No observable change in XRD patterns is found between the un-annealed and post-ELA films. Conversely, the noticeable diffraction peaks of post-ELA + RTA films indicate that the crystallinity of post-ELA films is improved after subsequent RTA. The intensities of (100), (110) and (211) orientations increase as the annealing temperature of subsequent RTA increases.

Figure 8 shows the cross-sectional TEM images and selected-area diffraction patterns (SADPs) to investigate the

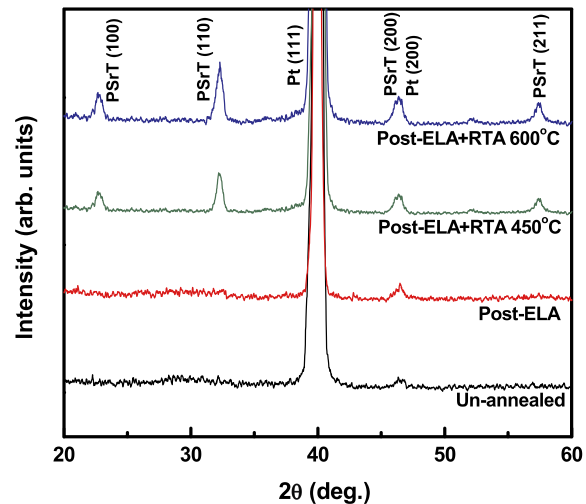

FIGURE 7 X-ray diffraction patterns of PSrT films un-annealed, post-ELA, and post-ELA + RTA at (**b**) 450 °C and (**c**) 600 °C

microstructure of post-ELA + RTA films. The bright-field (BF) image of PSrT film indicates that microstructure is divided into two regions (Fig. 8a). The upper region can be connected to the initial crystal seed induced by ELA (Fig. 5) and followed by grain growth during subsequent RTA (Fig. 7). Moreover, the SADPs show that area A and area B are crystalline. The coarsening of the grain during subsequent RTA could be limited by the existed grain boundaries induced by post-ELA. This may be the reason why the microstructure is divided into two regions. The central dark-filed (CDF) images (Fig. 8b) of $(200)_{PSRT}$ and $(110)_{PSrT}$ diffraction spots were also in agreement with the result. It is seen that the large grain is existed in the lower region, which is associated with the nucleation from the underneath amorphous region and grain coarsening during subsequent RTA. In contrast, the small grain located in the upper region could be attributed to the coarsening limited by existed grain boundaries. Furthermore, the preferred orientations of grains located in the upper or lower regions are also influenced by post-ELA + RTA. Nevertheless, the evolution of microstructure and crystallinity of films after ELA + RTA is not clear at present.

Figure 9 reveals AES depth profiles of PSrT films deposited on $Pt/Ti/SiO_2/Si$ substrate after ELA and ELA + RTA at 600 °C. Without standard samples to calibrate the sensitivity factor, the count intensity of elements presented here can only correspond to relative elemental concentrations. The post-ELA film shows a sharp interface between the PSrT film and Pt electrode (Fig. 9a). Nonetheless, slight diffusion of Ti, Sr and Pb elements from films to Pt electrode is observed after ELA + RTA (Fig. 9b).

Figure 10a shows the *C–E* hysteresis loops of PSrT films un-annealed, post-ELA and post-ELA + RTA at 450 and 600 °C. It indicates that the distinct *C–E* hysteresis loops can be obtained for films after ELA and ELA + RTA. The larger capacitance and better ferroelectricity can be obtained by subsequent RTA at higher temperature. Figure 10b demonstrates the corresponding dielectric constants extracted from the zero-field capacitance. It is observed that the dielectric constant of films can be slightly increased by post-ELA and greatly increased after RTA. The large dielectric constant

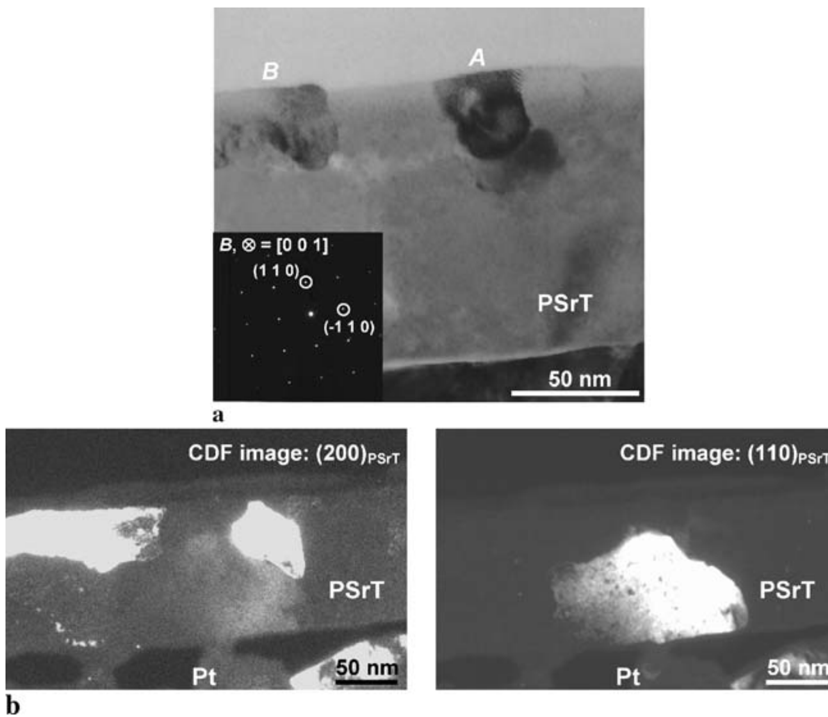

FIGURE 8 (**a**) Cross-sectional TEM image, selected-area diffraction patterns (SADPs) and (**b**) central dark-filed (CDF) images of $(200)_{PSRT}$ and $(110)_{PSrT}$ diffraction spots for PSrT films post-ELA + RTA at 600 °C

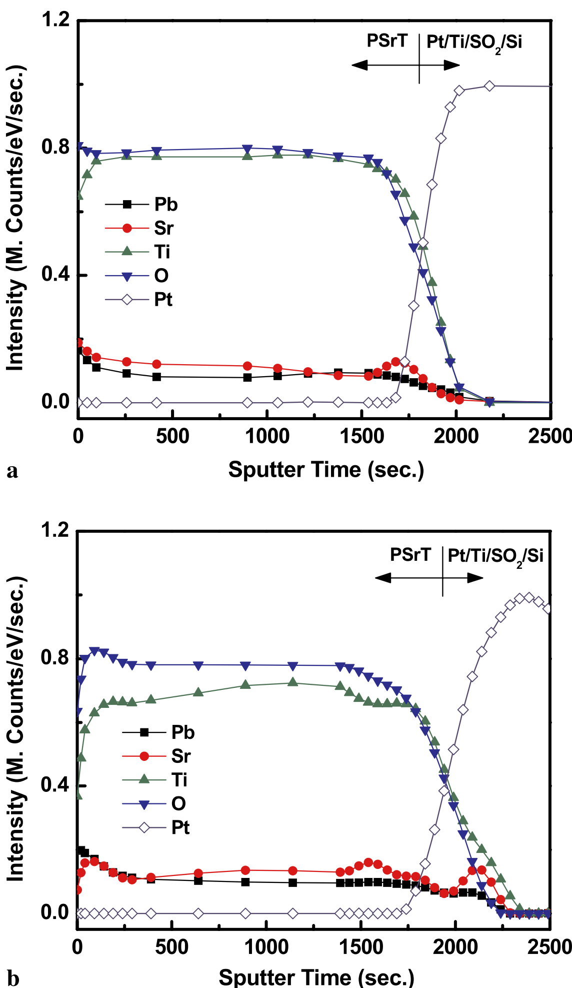

FIGURE 9 AES depth profiles of PSrT films deposited on $Pt/Ti/SiO_2/Si$ substrate (**a**) post-ELA and (**b**) post-ELA + RTA at 600 °C

can be found for post-RTA and post-ELA + RTA films at high annealing temperatures. In general, post-ELA + RTA films exhibit higher dielectric constant (e.g., 325 and 492 at 450 °C and 600 °C, respectively) than post-RTA films (e.g., 81 and 387 at 450 °C and 600 °C, respectively). Furthermore, the trend of dielectric constant is compatible with the results of XRD and GIAXRD (Figs. 2, 5, and 7) Thus, the dielectric properties and ferroelectricity of films are obviously dependent on the crystallinity, which are influenced by the annealing condition.

Figure 11a shows the *J–E* characteristics of films un-annealed, post-ELA and post-ELA + RTA at 450 and 600 °C. It reveals that the leakage current increases after ELA and ELA + RTA. The leakage current becomes larger after ELA + RTA at higher annealing temperature, which is analogous with that of post-RTA films. The result could be attributed to the formation of Pb and oxygen vacancies and interfacial diffusion (Fig. 9) at high temperatures. Figure 11b compares the leakage current density biased at +100/+150 kV/cm for PSrT films un-annealed, post-ELA, post-RTA and post-ELA + RTA at 450 and 600 °C. The leakage current density of films is a function of applied biases and annealing conditions. It is observed that the leakage current density of post-ELA + RTA films at 600 °C is inhibited (i.e., 0.97 and 9.55 $\mu A/cm^2$ at +100 and +150 kV/cm, accordingly) and 1.7–2.4 orders of magnitude smaller than that of post-RTA films at 600 °C (i.e., 238 and 454 $\mu A/cm^2$ at +100 and +150 kV/cm, accordingly).

Figure 12 shows the characteristics of time-dependent dielectric breakdown (TDDB) to predict the 10 year lifetime. TDDB is regarded as the resistance degradation of dielectric films, which increases the leakage current slowly under constant temperature and dc field stress. The mechanism of resistance degradations in perovskite films could be categorized into the grain boundary model and the reduction

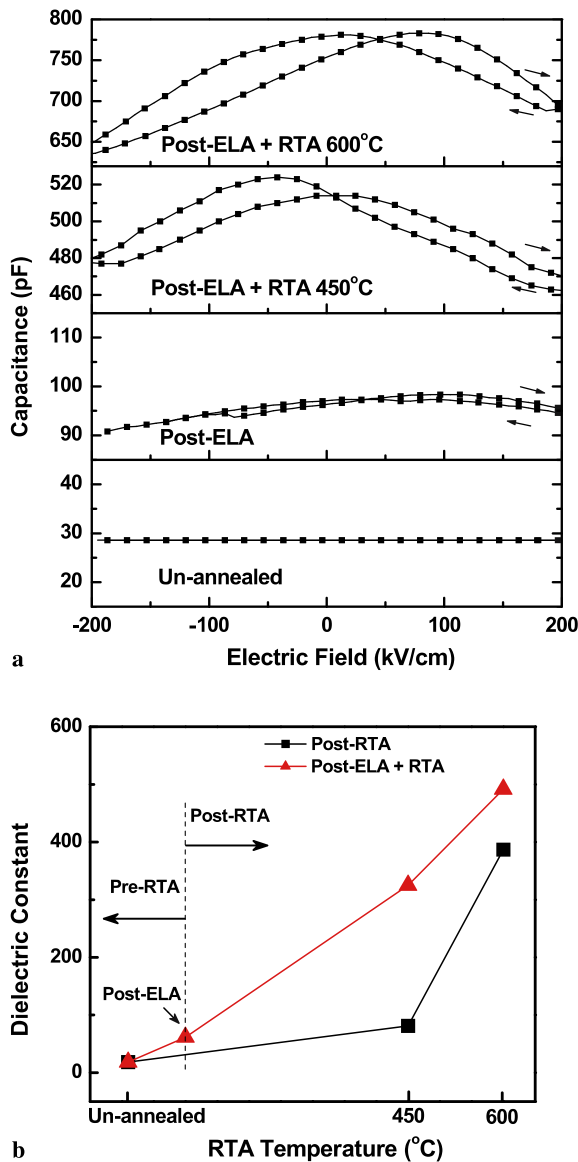

FIGURE 10 (**a**) Capacitance versus electric field (C–E) hysteresis loops of PSrT films un-annealed, post-ELA and post-ELA + RTA at 450 and 600 °C. (**b**) The corresponding dielectric constants of PSrT films un-annealed, post-ELA, post-RTA and post-ELA + RTA at 450 and 600 °C

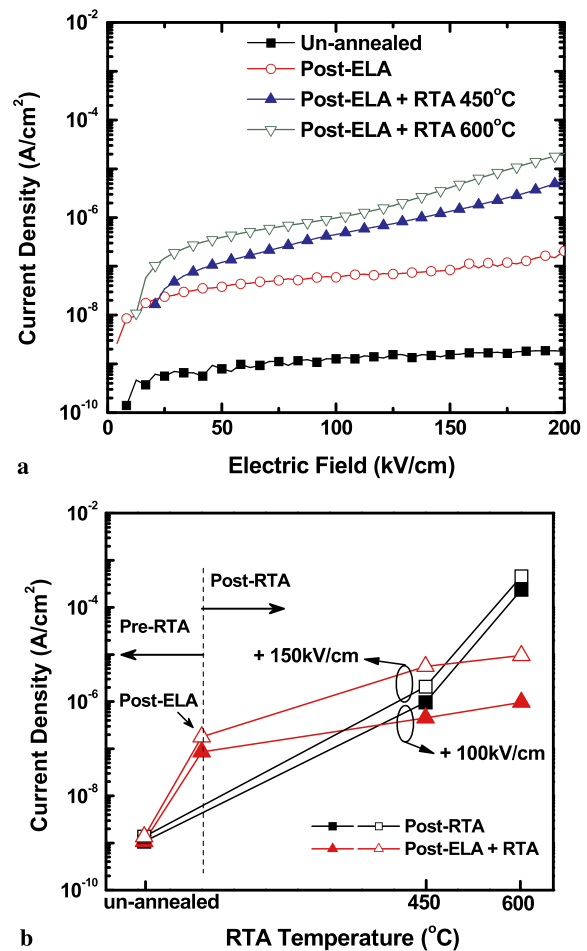

FIGURE 11 (**a**) Current density versus electric field (J–E) characteristics of PSrT films un-annealed, post-ELA and post-ELA + RTA at 450 and 600 °C. (**b**) The comparison of leakage current density biased at +100/+150 kV/cm for PSrT films un-annealed, post-ELA, post-RTA at 450 and 600 °C, and post-ELA + RTA at 450 and 600 °C

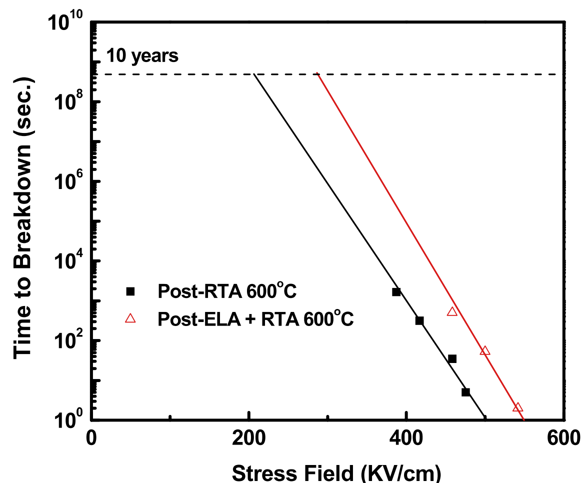

FIGURE 12 TDDB characteristics (time to breakdown as a function of stress field) of PSrT films post-RTA and post-ELA + RTA at 600 °C

model [19–21]. A large potential barrier across the grain boundary will result in shared drop in voltage and suppress resistance degradation. On the other hand, the reduction model suggests that oxygen vacancies and injection electrons cause resistance degradation. Since post-ELA was conducted in oxygen ambient and could reduce the oxygen vacancies on the film surface (not shown in this work). Therefore, post-ELA + RTA PSrT films exhibit the longer lifetime and higher breakdown field due to their smaller leakage current density (Fig. 11b).

4 Conclusions

The surface morphologies, crystallinity, microstructure, and electrical characteristics of PSrT films are found to be dependent on the annealing condition. The un-annealed film is amorphous and does not exhibit C–E hysteresis loops. After ELA, the PSrT film shows a dense surface with enhanced crystallinity in the upper region of films, resulting in the slight increase of the dielectric constant and leakage current. PSrT films after RTA reveal perovskite structures

and C–E hysteresis loops, suggesting that the ferroelectricity is improved. However, after RTA at high temperature, the PSrT film shows pin holes on the surface and interfacial diffusion between layers, which leads to a large leakage current. Furthermore, the film after laser-assisted two-step annealing exhibits good crystallinity, large C–E hysteresis loops, high dielectric constant, and low leakage current density. In summary, the laser-assisted two-step annealing (post-ELA + RTA) provides a way to improve the electrical properties and reliability of PSrT films, which shows better characteristics than single-step annealing (e.g., ELA or RTA).

ACKNOWLEDGEMENTS This work was supported in part by the National Science Council of ROC under the contract NSC95-2221-E-009-253. Thanks are also due to the Nano Facility Center (NFC) in National Chiao Tung University and the National Nano Device Laboratory (NDL) of the NSC for the technical supports.

REFERENCES

1 D.H. Kang, J.H. Kim, J.H. Park, K.H. Yoon, Mater. Res. Bull. **36**, 265 (2001)
2 F. Zhang, T. Karaki, M. Adachi, Japan. J. Appl. Phys. **44**, 6995 (2005)
3 T. Karaki, M. Adachi, Japan. J. Appl. Phys. **44**, 692 (2005)
4 C.C. Chou, C.S. Hou, G.C. Chang, H.F. Cheng, Appl. Surf. Sci. **142**, 413 (1999)
5 C.C. Chou, C.S. Hou, H.F. Cheng, Ferroelectrics **206–207**, 393 (1998)
6 C.S. Hou, H.C. Pan, C.C. Chou, H.F. Cheng, Ferroelectrics **232**, 129 (1999)
7 D. Roy, S.B. Krupanidhi, J. Mater. Res. **7**, 2521 (1992)
8 C.P. De Araujo, J.F. Scott, G.W. Taylor, *Ferroelectric Thin Films, Synthesis and Basic Properties, Ferroelectric and Related Phenomena* (Gordon and Breach Publishers, New York, 1996), vol. 10, pp. 193–226 and pp. 447–478
9 D.G. Lim, Y. Park, S.I. Moon, J. Yi, Applications of Ferroelectrics 2000, ISAF 2000, Proc. 2000 12th IEEE Int. Symposium, Honolulu, 599 (2000)
10 W. Huang, S.W. Jiang, Y.R. Li, J. Zhu, Y. Zhang, X.H. Wei, H.Z. Zeng, Thin Solid Films **500**, 138 (2006)
11 S. Kuchipudi, H.C. Lee, J.H. Hunag, I.N. Lin, Ferroelectrics **328**, 33 (2005)
12 H.C. Cheng, C.C. Tsai, J.H. Lu, H.H. Chen, B.T. Chen, T.K. Chang, C.W. Lin, J. Electrochem. Soc. **154**, J5 (2007)
13 A. Marmorstein, A.T. Voutsas, R. Solanki, J. Appl. Phys. **82**, 4303 (1997)
14 Y. Zhu, J. Zhu, Y.J. Song, S.B. Desu, Appl. Phys. Lett. **73**, 1958 (1998)
15 C.F. Chou, H.C. Pan, C.C. Chou, Japan. J. Appl. Phys. **41**, 6679 (2002)
16 D.C. Shye, B.S. Chiou, C.C. Hwang, C.C. Jaing, H.W. Hsu, J.S. Chen, H.C. Cheng, Japan. J. Appl. Phys. **42**, 1680 (2003)
17 D.B. Chrisey, G.K. Huber, *Pulsed Laser Deposition of Thin Films* (Wiley, New York, 1994), pp. 55–87 and pp. 167–198
18 B.H. Park, S.J. Hyun, C.R. Moon, B.D. Choe, J. Lee, C.Y. Kim, W. Jo, T.W. Noh, J. Appl. Phys. **84**, 4428 (1998)
19 R. Waster, R.T. Baiatu, K.H. Haratl, J. Am. Ceram. Soc. **73**, 1645 (1990)
20 M.S. Tsai, T.Y. Tseng, IEEE Trans. Comp. Packag. Technol. **23**, 128 (2000)
21 J.L. Wang, Y.S. Lai, B.S. Chiou, H.Y. Tseng, C.C. Tsai, C.P. Juan, C.K. Jan, H.C. Cheng, J. Phys.: Condens. Matter **18**, 10 457 (2006)